ELSEVIER

International Journal of Heat and Fluid Flow 20 (1999) 187–195

International Journal of HEAT AND FLUID FLOW

www.elsevier.com/locate/ijhff

Use of direct numerical simulation to study the effect of Prandtl number on temperature fields

Yang Na [a], Dimitrios V. Papavassiliou [b], Thomas J. Hanratty [a,*]

[a] *University of Illinois at Urbana-Champaign, 205 R. Adams Lab., Department of Chemical Engineering, 600 South Mathews Avenue, Box C-3, Urbana, IL 61801-3792, USA*

[b] *Mobil Technology, Upstream, SRC, Dallas, TX 75244, USA*

Abstract

The influence of Prandtl number on statistical parameters characterizing turbulent transport and the spatial variation of the mean-square of the temperature fluctuations, $\overline{\theta^2}$, is described. The system considered is fully developed flow in a channel for which the bottom wall is heated and the top wall is cooled. Results from direct numerical solutions of the Euler balance equations for $Pr = 0.3$, 1, 3, 10 and Lagrangian studies, in a DNS, of the dispersion of heat markers from wall sources for $Pr = 0.1$–2400 are used. The Eulerian results for $Pr = 10$ are new and of particular interest. A time scale τ_θ can be defined from the dissipation of $k_\theta = \overline{\theta^2}/2$, as $\tau_\theta = k_\theta/\epsilon_\theta$. This is analogous to the time scale defined from the dissipation of turbulent kinetic energy, $\tau = k/\epsilon$. Prandtl number is found to strongly affect τ_θ and the correlation, $\overline{u_i\theta}/(\overline{u_i^2})^{1/2}(\overline{\theta^2})^{1/2}$. These results can be understood by recognizing that the spectral density function for temperature fluctuations extends over an increasingly larger range of wavenumbers as Pr increases. The observed effect of Pr on τ_θ suggests fundamental problems in developing relations for the turbulent diffusivity by a $k_\theta\tau\tau_\theta$ approach analogous to the $k\tau$ approach used to describe momentum transport. The use of a gradient transport model to represent the turbulent transport of k_θ also has fundamental problems.

Keywords: Heat transfer; Direct numerical simulation; Turbulent diffusivity; Prandtl number

Notation

c_p	specific heat at constant pressure
D	molecular diffusivity
D^t	turbulent diffusivity
H	half channel height
K	mass transfer coefficient
k	turbulent kinetic energy or fluctuating mass transfer coefficient
k_x	streamwise wavenumber
k_θ	half the mean-square temperature fluctuations
n	exponent that describes the variation of D^t with the distance from the wall
P	pressure
P_x	streamwise pressure gradient
P_θ	production of $\overline{\theta^2}$
Pr	Prandtl number
Pr^t	turbulent Prandtl number
q	local heat flux
q^2	$u^2 + v^2 + w^2$
q_w	heat flux at the channel wall
$R_{\theta u}$	correlation coefficient of θ and u
$R_{\theta v}$	correlation coefficient of θ and v
Sc	Schmidt number
T	temperature
$\overline{T}$	mean temperature
T_w	temperature at the wall
T^*	friction temperature
t	time
$\mathbf{u}$	velocity vector
$u,\ v,\ w$	fluctuating velocity components in the $x,\ y,\ z$ directions
u_τ	friction velocity
$W_{\theta\theta}$	spectral density function for $\overline{\theta\theta}$
$W_{\theta v}$	co-spectral density function for $\overline{\theta v}$
$x,\ y,\ z$	streamwise, normal and spanwise coordinates
y_w	distance from the lower wall made dimensionless by wall variables
w	weight function

Greek

Δ_θ	thickness of conductive layer
ϵ	dissipation of turbulent kinetic energy
ϵ_θ	dissipation of temperature fluctuations
$\tilde{\epsilon}_\theta$	$\epsilon_\theta - 1/\mathrm{Pr}(\partial(\overline{\theta^2})^{1/2}/\partial y)^2$
κ_θ	von Karman constant for temperature
λ_x	Taylor microscale for temperature in the x direction
λ_y	Taylor microscale for temperature in the y direction

* Corresponding author. E-mail: hanratty@aries.scs.uiuc.edu.

0142-727X/99/$ – see front matter
PII: S0142-727X(99)00008-9

λ_z	Taylor microscale for temperature in the z direction
λ_θ	Taylor microscale defined by $1/\lambda_\theta^2 = 1/\lambda_x^2 + 1/\lambda_y^2 + 1/\lambda_z^2$
ν	kinematic viscosity
ν^t	turbulent kinematic viscosity
ω	vorticity vector
Π	pseudo pressure
ρ	fluid density
σ	standard deviation
τ	time scale of velocity field
τ_θ	time scale of temperature field
θ	fluctuating temperature

1. Introduction

The principal theoretical problem in turbulent transport is to relate local rates and temperature fluctuations to the properties of the fluctuating velocity. The classical approach has been to use the analogy which assumes the eddy diffusivity of heat, D^t, is proportional to the eddy kinematic viscosity, ν^t. The implementation of this approach requires the prediction of the turbulent Prandtl number, $Pr^t = \nu^t/D^t$. The modelling of Pr^t has often involved the utilization of the dissipation of the variance of the temperature fluctuations, $\overline{\theta^2}/2 = k_\theta$, in a framework that mimics the use of k in the k/ϵ equation for momentum transport (Launder, 1978; Nagano and Kim, 1988; Youssef et al., 1992). Another approach has been to develop an equation for the scalar transport term, $\overline{\theta u_i}$ (Launder and Samaraweera, 1979; Nagano and Tagawa, 1988 ; Nagano and Tagawa, 1990). A critical test for models of scalar-transport is their ability to predict the influence of Prandtl number on statistical parameters that appear in the equations describing the system.

With advance of large scale computers, several direct numerical simulations of turbulent channel flow with heat transfer were carried out (Kim and Moin, 1989; Kasagi and Ohtsubo, 1993; Kawamura et al., 1997; Kawamura and Abe, 1998; Wikstrom and Johansson, 1998) for $Pr \leqslant 5$ with different types of thermal boundary condition. This laboratory also has been addressing the question raised above by studying fully developed heat transfer in a channel in which the bottom wall is heated and the top wall is cooled at the same rate so that both walls are kept at constant temperatures (T_w and $-T_w$). Since the velocity and temperature fields are fully developed, the heat fluxes at different distances from the bottom wall are the same. Direct numerical simulations of the Eulerian balance equations for $Pr = 0.05$–10 have been performed. Lagrangian studies have been carried out that involve the study of the dispersion of heat markers from wall sources characterized by $Pr = 0.1$–2400. This paper gives an account of these studies. Particularly noteworthy are the recently developed DNS for $Pr = 10$ and the demonstration that Lagrangian methods can be used at arbitrarily large Pr.

Results are presented for the turbulent diffusivity, for the terms in the balance equation for k_θ, for the correlation coefficients, $\overline{\theta u_i}/(\overline{\theta^2})^{1/2}(\overline{u_i^2})^{1/2}$, and for the timescale defined from the thermal dissipation, $\tau_\theta = (\overline{\theta^2}/2)/\epsilon_\theta$. An understanding of the influence of Pr on these quantities needs to recognize that the spectral density function for $\overline{\theta^2}$ extends over an increasing range of wavenumbers as Pr is increased. An important conclusion is that the use of τ_θ in developing models for the temperature field is flawed.

2. Methodology

2.1. Eulerian approach

Numerical solutions are obtained for the three-dimensional, time-dependent Navier–Stokes equation in a skew-symmetric form and the advection–diffusion equation.

$$\frac{\partial \mathbf{u}}{\partial t} = (\mathbf{u} \times \boldsymbol{\omega}) - \nabla \Pi - P_x \mathbf{e}_x + \nabla^2 \mathbf{u}, \tag{1}$$

$$\frac{\partial T}{\partial t} = \mathbf{u} \cdot \nabla T + \frac{1}{\mathrm{Pr}} \nabla^2 T, \tag{2}$$

where

$$\boldsymbol{\omega} = \nabla \times \mathbf{u}, \tag{3}$$

$$\Pi = P - P_x x + (\mathbf{u} \cdot \mathbf{u})/2 \tag{4}$$

and $\mathbf{u}$ and P denote the velocity vector and the static pressure. All variables are made dimensionless by using wall variables. Solutions of Eqs. (1) and (2) are obtained, which are periodic in the streamwise and spanwise directions, by using the algorithm described by Lyons et al. (1991). The Reynolds number based on the friction velocity and the half-channel height, H, is 150. In presenting the results, x, y, z and u, v, w represent coordinates and velocity components in the streamwise, the wall-normal and the spanwise directions.

The results for $Pr = 10$ are for an x, y, z grid of $128 \times 193 \times 128$. The resolution in the y-direction varied from $\Delta y = 0.02$ at the wall to $\Delta y = 2.45$ at the center of the channel. The resolutions in the x and z directions were $\Delta x = 15$, $\Delta z = 7.5$. Preliminary computations were conducted on a coarse grid and the flow field was interpolated onto the $128 \times 193 \times 128$ grid. A time of about 800 ν/u_τ^2 was required to reach a stationary state and the averaging time was 715 ν/u_τ^2. Averaging was also carried out in the x and z directions so the statistics vary only with y. A memory of 2 gigabytes was required on a HP/Convex-X. Computer runs were also carried out with grids of $128 \times 257 \times 128$ and $128 \times 193 \times 256$ to ensure adequacy of the resolution. These computations were performed for long enough time to get reasonable mean statistics up to second order. The results show the following: (a) A wall-normal resolution of 193 grids is required; higher resolution in this direction improves calculations of the mean temperature and the root-mean square of the temperature fluctuations only slightly (peak rms temperature fluctuations differ by 1.6%). (b) The use of a higher resolution in the spanwise direction (256 grid points) does not produce significant changes in the first-order statistics.

The results presented in this paper for $Pr = 0.3$, 1 and 3 were obtained for a $128 \times 129 \times 128$ grid for which Δy varied from 0.045 to 3.68. A time of about 1000 was needed to reach a stationary state; averaging was done over time periods of 775, 750, 370 ν/u_τ^2 for $Pr = 0.3$, 1.0 and 3.0, respectively. A memory of 0.7 gigabytes was needed on a HP/Exemplar-S.

A principal focus of this paper is the comparison of calculations with $Pr = 1$, 3 and 10. For low Peclet numbers, equal to the product of Re and Pr, the turbulent diffusivity is qualitatively different from what is found for large Pe, in that molecular diffusion is causing the turbulent diffusivity to decrease because of "leakage" of thermal tags from eddies (Kontomaris and Hanratty, 1994). Because of the low values of Pe used in the DNS, this becomes important for $Pr = 0.3$, for which the ratio of the molecular diffusivity to the turbulent diffusivity is about 1/3.

2.2. Lagrangian calculations

The trajectories of heat markers released at time t_0 from an infinitesimal source on the wall were calculated in a DNS of channel flow. The Reynolds number based on the half-height of the channel and the friction velocity was 150. The calculations were done with an x, y, z grid of $128 \times 65 \times 128$. The particle tracking method developed by Kontomaris et al. (1992) was used. Each marker moves due to convective and to molecular effects. The convective part of the motion is calculated from the fluid velocity at the marker position. The effect of molecular diffusion is simulated by imposing a three-dimensional random walk on the particle motion; it is added to the convective part of the motion after each time step, Δt, and takes values from a Gaussian distribution with zero mean and standard deviation $\sigma = (2\Delta t/\mathrm{Pr})^{1/2}$, in wall units (Papavassiliou and Hanratty, 1995; Kontomaris and Hanratty, 1994). A total of 16,128 markers were released on a 127×127 grid that covered the bottom wall. The behavior of the markers was followed over a time period of 2750 wall units. A time step of $\Delta t = 0.25$ was used.

The experiments with instantaneous sources provide the probability function, $P_1(x - x_0,\ y,\ t - t_0)\ \mathrm{d}x_0\ \mathrm{d}t_0$. A physical interpretation of P_1 is that it represents the evolution in time of the ensemble average of markers released instantaneously from a line source at the wall. Since the flow field is homogeneous in the x and z directions, there is no statistical dependence on the initial location of the point sources.

Probability P_1 can be used to obtain information about the behavior of a continuous line source at x_0 by integrating over time.

$$P_2(x - x_0, y) = \int_0^\infty P_1(x - x_0, y, t - t_0)\ \mathrm{d}(t - t_0). \tag{5}$$

The distribution of mean temperature over a plane source is

$$\overline{T}(x, y) = \int_0^x P_2(x - x_0,\ y)\ \mathrm{d}(x - x_0). \tag{6}$$

The temperature field from a heated bottom wall and a cooled top wall is then given as

$$\overline{T}(x, y) = \int_0^x [P_2(x - x_0, y) - P_2(x - x_0, -y)]\ \mathrm{d}(x - x_0), \tag{7}$$

where y is the distance from the center of the channel. A fully developed temperature profile is obtained by letting $x \to \infty$.

The Eulerian simulations used $T_\mathrm{w} = \text{constant}$ as the boundary conditions for the mean temperature at the wall. In order to compare Lagrangian results with the Eulerian results, a weight function, $w(t)$, needs to be introduced so that the number of markers at the wall remains constant throughout the time integration. Eq. (7) thus becomes

$$\overline{T}(x, y) = \int_0^\infty \int_0^x w(t - t_0) P_1(x - x_0, y, t - t_0) d(x - x_0)\ \mathrm{d}(t - t_0) \tag{8}$$

with

$$w(t - t_0) = \frac{T_\mathrm{w} - T(y = -h, t - t_0)}{T_\mathrm{w}}. \tag{9}$$

3. Results from Lagrangian method

Results from the Lagrangian analysis have been presented by Papavassiliou and Hanratty, 1995; Papavassiliou and Hanratty, 1997. This section gives a brief review of the findings, in order to enhance the discussion of the effects of Pr on statistical properties of the temperature field. Fig. 1 shows a typical path for a thermal marker with $\mathrm{Pr} = 100$, that started at the wall, $y = -H/2$, $t = t_0$. The ordinate is the dimensionless time, t, and y_w is the dimensionless distance from the wall. At small times the markers move away from the wall by molecular diffusion. Eventually they become entrained in the turbulence and turbulent motions dominate their dispersion from the wall. The distance from the wall at which the marker becomes entrained in the turbulence increases with decreasing Prandtl number. Three zones are observed: a region where molecular diffusion dominates, a region where there is an interaction between molecular and turbulent diffusion, a region where turbulent diffusion dominates. For very small Prandtl numbers only the first two regions are present. Fig. 2 shows the average locations at two different times of a large number of $\mathrm{Pr} = 1$ markers that originate at the wall at $t = 0$. This clearly shows that a specific region of space will be primarily affected by markers released over a specific time interval.

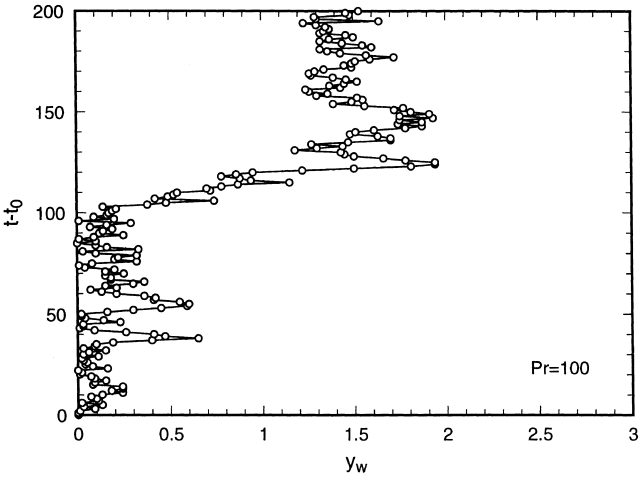

Fig. 1. Typical trajectory for a thermal marker with $\mathrm{Pr} = 100$.

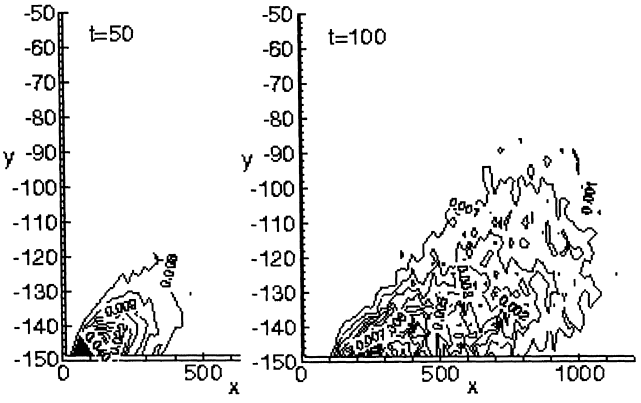

Fig. 2. Spatial distributions of $\mathrm{Pr} = 1$, heat markers released at the wall at $t = 0$.

Results such as these can be used to calculate the average temperature field at a given distance downstream, x, from the entrance of a section where heat is added to the fluid from the bottom wall at a constant rate and removed from the top wall at the same rate. For large enough x the average temperature field, calculated in this way, reaches a fully developed condition. This analysis was used to calculate the mass transfer coefficients, made dimensionless with the friction velocity, that are presented in Fig. 3.

Results from three separate laboratory studies in a pipe at $Sc = 2400$ are also presented, as are results from the DNS. In studies with the DNS, the temperature driving force is defined as the difference between the temperature of the bottom wall and the bulk temperature in the bottom half of the channel [rather than the centerline temperature as used by Papavassiliou and Hanratty (1997)]. The Lagrangian calculations agree closely with the laboratory measurements and with Eulerian calculations. The straight line represents the relation developed by Shaw and Hanratty (1977) from their measurements of mass transfer in a pipe over a range of Schmidt numbers of 693 to 39,300. The Lagrangian calculations of mass transfer rates and eddy transport coefficients (Papavassiliou and Hanratty, 1997) support the controversial suggestion of Shaw and Hanratty that $K \sim Sc^{-0.704}$ at large Sc, rather than as $Sc^{-2/3}$ or $Sc^{-3/4}$. They are represented by $D^t \sim y^{3.38}$ for large Pr, rather than y^3. The results from the DNS at smaller Pr, however, are represented by $K \sim Sc^{-0.546}$. Interpretations of the results at large Sc have been presented by Campbell and Hanratty (1983) and by Hanratty and Vassiliadou (1988).

An interesting comparison between the Lagrangian and Eulerian computations can be made. Both use the turbulent velocity field obtained from a DNS. For the present, the Eulerian calculation is limited to $Pr \leqslant 10$. However the Lagrangian calculation can be done for arbitrarily large Pr. Another result (Papavassiliou and Hanratty, 1997) coming from Lagrangian calculations is that the spatial variation of the turbulent diffusion coefficient observed in the Eulerian analysis is not entirely due to spatial variations of the turbulence – but is strongly affected by the time-dependency of turbulent diffusion. Many aspects of the physics of turbulent transport are understood more clearly with the Lagrangian analysis for the simple case of turbulent flow in channel. To complete this theoretical approach one needs to develop a model for diffusion from a wall source.

4. Results from Eulerian calculations

4.1. Mean temperatures

Mean temperatures, obtained from the Eulerian calculations, are shown in Fig. 4 for $Pr = 1$, 3 and 10. The abscissa is the distance from the center of the channel made dimensionless with the half height. The ordinate is the mean temperature relative to the centerline temperature divided by the absolute value of the difference of the wall temperature and the centerline temperature. Lagrangian results for $Pr = 1,10$ are also presented for comparison. The good agreement provides support for the accuracy of the Eulerian calculations. Fig. 5 is a semi-logarithmic plot in which the abscissa is the distance from the bottom wall made dimensionless with the friction velocity and the kinematic viscosity. The ordinate is the difference between the local mean temperature and the wall temperature made dimensionless with the friction temperature, $T^* = q_w/\rho c_p u_\tau$. Even though an extensive well-defined logarithmic layer is not expected, straight lines represented by the equation

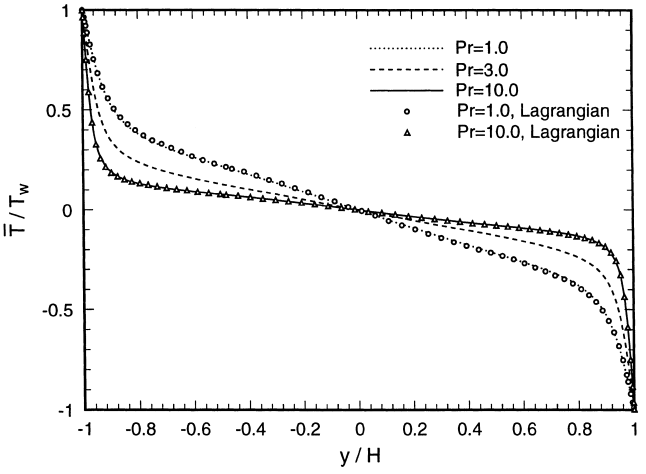

Fig. 4. Comparison of mean temperature profiles.

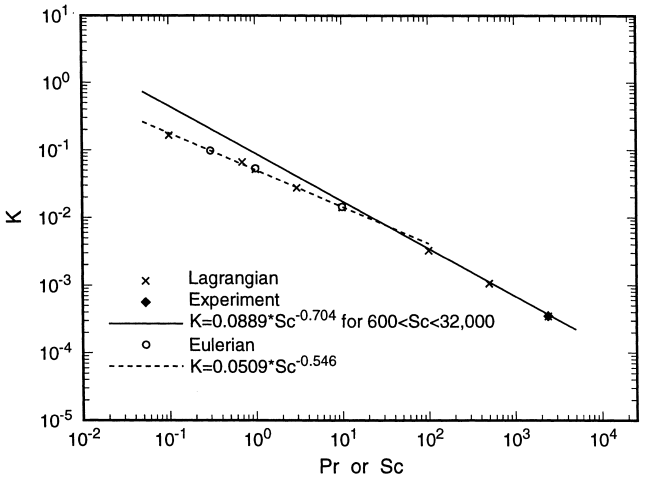

Fig. 3. Comparison of values of K obtained by Eulerian and Lagrangian methods. The line indicates measurements for large Sc.

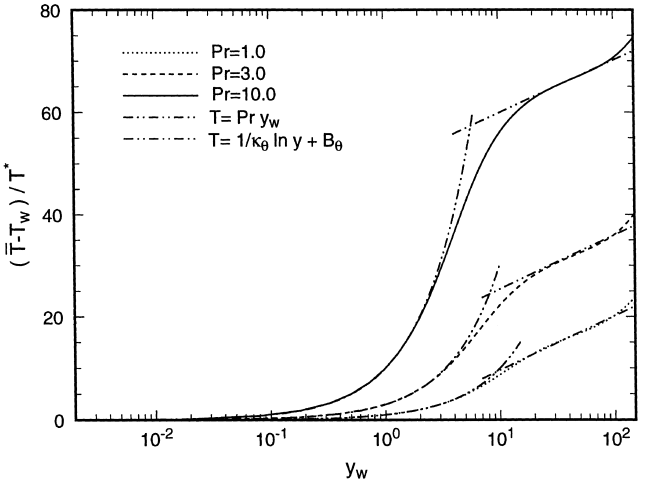

Fig. 5. Mean temperature profiles in semi-log coordinate.

$$\frac{\overline{T}-T_w}{T^*}=\frac{1}{\kappa_\theta}\ln y_w+B_\theta \tag{10}$$

are presented, where $\kappa_\theta=0.22$, 0.21, 0.23 and $B_\theta=-1.0$, 14.7, 49.5 for $Pr=1$, 3, 10. It is noted that the slope $1/\kappa_\theta$ is approximately constant for the Pr considered. These κ_θ are lower than the values of 0.48 obtained by Subramanian and Antonia (1981) for a turbulent boundary layer and 0.45 for measurements in an electrically heated pipe obtained by Johnk and Hanratty (1962). This difference in κ_θ is thought to be due to the thermal boundary condition at the wall and the much lower Reynolds number considered in the present work. A conductive sublayer exists close to the wall where turbulence is making a negligible contribution to the transfer of heat. Its thickness for $Pr=1$, 3, 10 is, respectively, $y_w=6.0$, 3.6, 1.9. Thus, the thickness of this layer, Δ_θ, varies as $Pr^{-1/2}$, over this range of Pr.

4.2. Balance equation for temperature variance

Measures of the magnitude of the temperature and velocity fluctuations are $\overline{\theta^2}$ and $\overline{q^2}=\overline{u^2}+\overline{v^2}+\overline{w^2}$. A balance equation for $k_\theta=\overline{\theta^2}/2$, analogous to the balance for $k=\overline{q^2}/2$, can be written as follows for fully developed flow in a channel:

$$0=-\overline{\theta v}\frac{dT}{dy}-\frac{1}{2}\frac{d(\overline{\theta^2 v})}{dy}+\frac{1}{Pr}\frac{d^2k_\theta}{dy^2}-\frac{1}{Pr}\left[\overline{\left(\frac{\partial\theta}{\partial x}\right)^2}+\overline{\left(\frac{\partial\theta}{\partial y}\right)^2}+\overline{\left(\frac{\partial\theta}{\partial z}\right)^2}\right], \tag{11}$$

where T and θ are the mean and fluctuating temperatures. All variables in this equation (and in subsequent discussions) are made dimensionless with the kinematic molecular viscosity, the friction velocity, u_τ, and the friction temperature, T^*. The terms in Eq. (11) are the production of k_θ, the turbulent transport of k_θ, the molecular transport of k_θ and the dissipation of k_θ, which has been designated as ϵ_θ. A sensitive test that a stationary state has been reached is when the sum of these terms equals zero. For $Pr=10$, the maximum imbalance, which occurs in the middle of the channel, is about 1.2% of the maximum production. As more samples are added, this imbalance decreases very slowly but the overall shapes of the curves representing terms in the budget hardly change.

Figs. 6 and 7 present values of $\overline{\theta v}$ and the production of temperature fluctuations, P_θ, for different Pr. As Pr increases, the heat flux by turbulent transport, $\overline{\theta v}$, becomes increasingly important near the wall. In the middle of the channel, the effect of molecular conductivity is relatively small and heat is mainly transported by the turbulence. Due to the finite temperature gradient (Fig. 4), the production does not go to zero in the middle of the channel. Sharp maxima in the production are noted close to the wall and a smaller broad maximum is obtained in the center of the channel. Fig. 8 presents calculations of the root mean-square of θ. Maxima correspond roughly with the maxima in the production of k_θ. Due to the increase in production with increasing y_w in the middle of channel, temperature fluctuations increase with y_w in this region for all Pr.

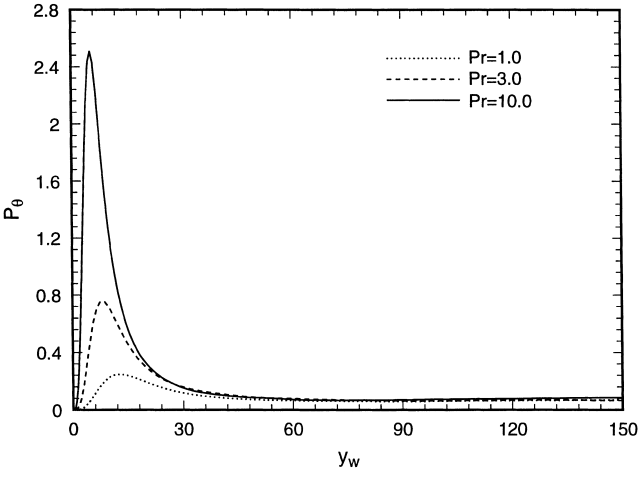

Fig. 7. Production of k_θ, P_θ.

Plots of the correlation coefficient $R_{\theta u}=\overline{\theta u}/(\overline{\theta^2})^{1/2}(\overline{u^2})^{1/2}$ and $R_{\theta v}=\overline{\theta v}/(\overline{\theta^2})^{1/2}(\overline{v^2})^{1/2}$ are presented in Figs. 9 and 10. The strong decrease of these correlations with increasing Pr is particularly noteworthy. As shown in Fig. 6, $\overline{\theta v}$ is higher for higher Pr throughout the channel. In order to understand the decrease in $R_{\theta v}$, it is useful to look at the behavior of $\overline{\theta v}$ and $\overline{\theta^2}$ in wavenumber space. Figs. 11 and 12 are the cumulative spectral density functions of $\overline{\theta v}$ and $\overline{\theta^2}$ versus wavenumber in the streamwise direction, k_x, at $y_w=25$. Plots of $\int_0^{k_x} W_{\theta\theta}\,dk_x$ show that the contribution from high wavenumbers to $\overline{\theta^2}$ increases in importance as Pr increases. However, its influence on the cumulative co-spectral density function for $\overline{\theta v}$ is relatively small. This is because high wavenumbers do not contribute significantly to $\overline{v^2}$, as they do to $\overline{\theta^2}$ at large Pr. Thus,

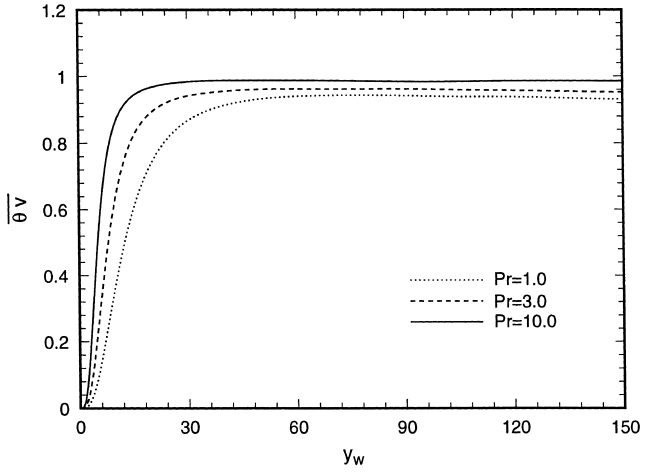

Fig. 6. Comparison of $\overline{\theta v}$.

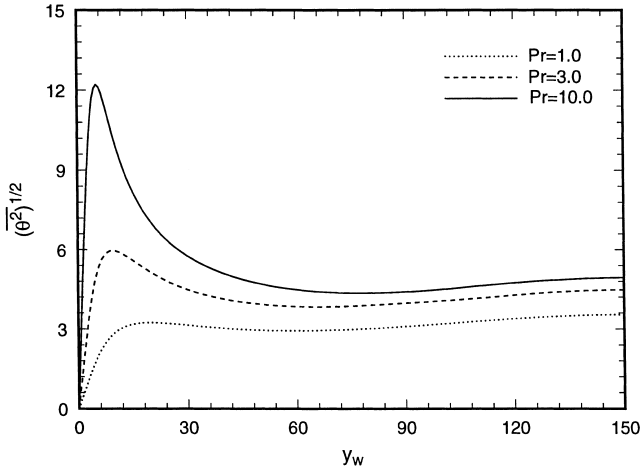

Fig. 8. Temperature fluctuations.

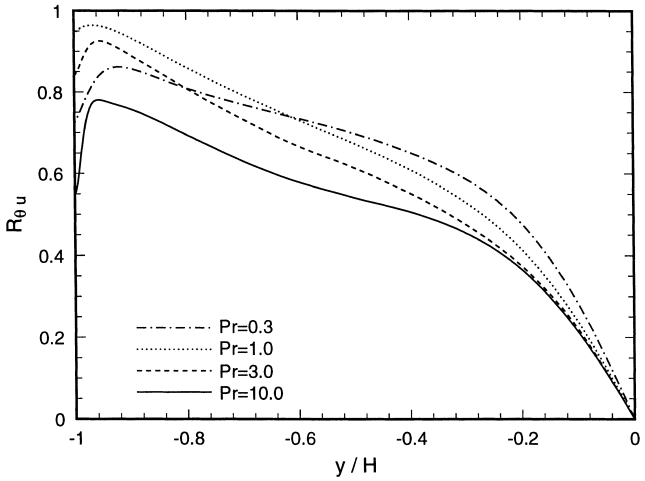

Fig. 9. Correlation coefficient $R_{\theta u}$.

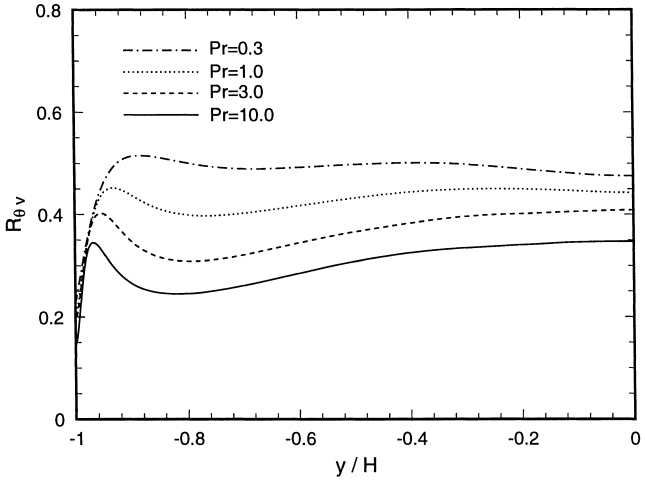

Fig. 10. Correlation coefficient $R_{\theta v}$.

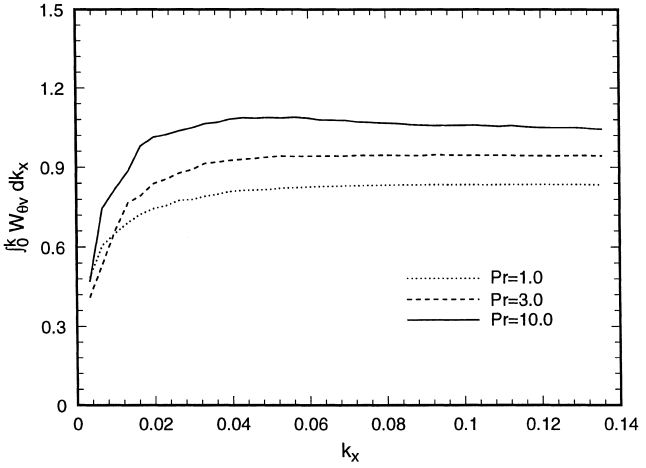

Fig. 11. Cumulative co-spectral density function of $\overline{\theta v}$ at $y=25$.

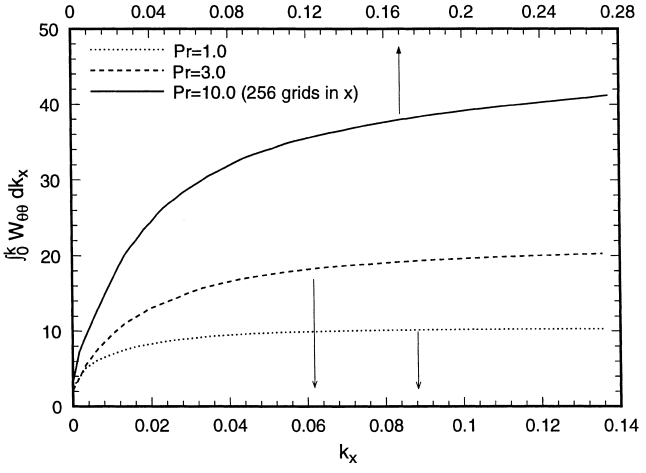

Fig. 12. Cumulative spectral density function of $\overline{\theta^2}$ at $y=25$.

the ratio of $\overline{\theta v}/(\overline{\theta^2})^{1/2}(\overline{v^2})^{1/2}$ decreases as Pr increases. It should be noted that the calculations for $\mathrm{Pr}=10$ in Fig. 12 used 256 grid points in the x-direction. This accounts for the larger range of k_x studied for this condition.

Calculations of ϵ_θ are presented in Fig. 13. The very high values close to the wall are in a region where the instantaneous temperature profiles are linear but oscillating in time. Usual practice is to define a term $\tilde{\epsilon}_\theta = \epsilon_\theta - 1/\mathrm{Pr}\left(\partial(\overline{\theta^2})^{1/2}/\partial y\right)^2$ which does not include the dissipation associated with these oscillations. Thus, the modified dissipation can be represented as follows:

$$\tilde{\epsilon}_\theta = \frac{1}{\mathrm{Pr}}\left[\overline{\left(\frac{\partial\theta}{\partial x}\right)^2} + \overline{\left(\frac{\partial\theta}{\partial z}\right)^2}\right] + \frac{1}{\mathrm{Pr}}\left[\overline{\left(\frac{\partial\theta}{\partial y}\right)^2} - \left(\frac{\partial\sqrt{\overline{\theta^2}}}{\partial y}\right)^2\right]. \tag{12}$$

Values of $\tilde{\epsilon}_\theta$ are presented in Fig. 14. One can use Eq. (12) to define a microscale, analogous to that defined by Taylor for the dissipation of turbulent energy,

$$\tilde{\epsilon}_\theta = \frac{1}{\mathrm{Pr}}\frac{\overline{\theta^2}}{2}\left(\frac{1}{\lambda_\theta^2}\right), \tag{13}$$

where

$$\frac{1}{\lambda_\theta^2} = \frac{1}{\lambda_x^2} + \frac{1}{\lambda_y^2} + \frac{1}{\lambda_z^2}. \tag{14}$$

The scale, λ_θ, is found to decrease with increasing Pr. The plot for $\mathrm{Pr}=0.3$, 1.0, 3.0, 10.0 in Fig. 15 shows, for a fixed Reynolds number, that $\lambda_\theta \sim \mathrm{Pr}^{-1/3}$. This result is consistent with Fig. 12 which shows that the contributions of high wavenumbers to $\overline{\theta^2}$ becomes more important with increasing Pr.

5. Results on turbulent diffusivity

A turbulent diffusivity of heat is defined as

$$\overline{\theta v} = D^{\mathrm{t}}\frac{\mathrm{d}\overline{T}}{\mathrm{d}y}. \tag{15}$$

This can be obtained from calculations of $\overline{\theta v}$ and $\mathrm{d}\overline{T}/\mathrm{d}y$. It can also be calculated from a knowledge of $\overline{T}(y)$ and the heat flux, q_{w}, at the wall. Since a fully developed condition is considered,

$$q(y) = q_{\mathrm{w}} = -(D + D^{\mathrm{t}})\frac{(\rho c_p \overline{T})}{\mathrm{d}y}. \tag{16}$$

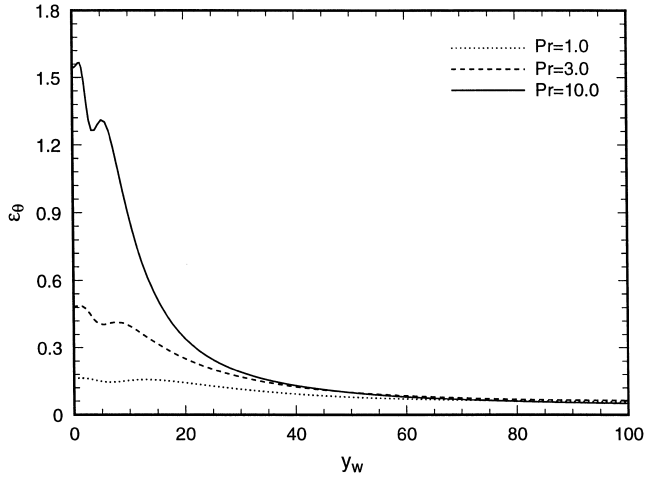

Fig. 13. Total dissipation of temperature field.

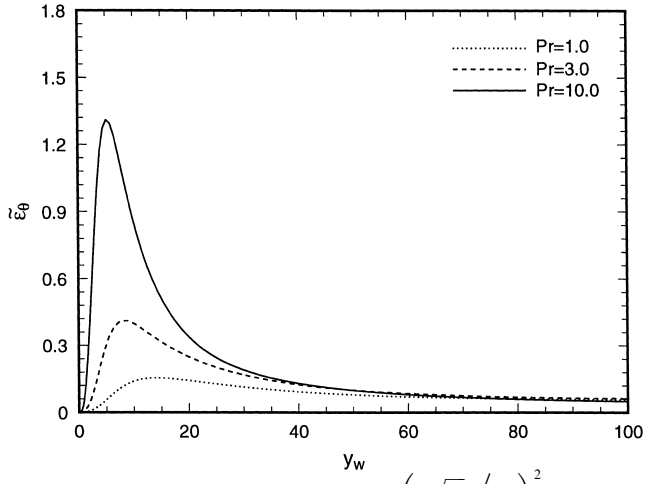

Fig. 14. Plot of $\tilde{\epsilon}_\theta = \epsilon_\theta - (1/\mathrm{Pr})\left(\partial\sqrt{\overline{\theta^2}}\Big/\partial y.\right)^2$.

If this is written in a dimensionless form,

$$1 = -\left(\frac{1}{\mathrm{Pr}} + D^{\mathrm{t}}\right)\frac{\mathrm{d}\overline{T}}{\mathrm{d}y}, \tag{17}$$

where D^{t} is made dimensionless with the molecular kinematic viscosity, $\overline{T}$, by the friction temperature and y, by the ratio of the kinematic viscosity to the friction velocity. In the Eulerian calculations the same value of D^{t} was obtained by Eqs. (15) and (17) after a stationary state was reached. In the Lagrangian calculation D^{t} was obtained from Eq. (17).

Values of D^{t} obtained from Eulerian calculations for $\mathrm{Pr} = 1$, 3, 10 are presented in Fig. 16, along with the values of the turbulent kinematic viscosity, ν^{t}, obtained for $H = 150$. The turbulent viscosity shown in this figure was calculated with a $128 \times 193 \times 128$ grid. It is noted in this plot that Pr is not having a strong effect on D^{t} for $\mathrm{Pr} \geqslant 1$. In the central regions of the channel slight differences are noted. These could be real, but they also could reflect computational issues. As can be seen in Fig. 4, the temperature gradient at the center of the channel decreases with increasing Pr so that the accuracy of the calculation becomes more important. Furthermore, the computations show that the central regions of the channel come to a stationary state slowly because the convection of temperature is influenced by large scale, small frequency velocity fluctuations. Thus, differences between the $\mathrm{Pr} = 1$ and $\mathrm{Pr} = 3$ calculations could have arisen because insufficient time was allowed to reach a stationary state for $\mathrm{Pr} = 3$. This does not seem to be the case for $\mathrm{Pr} = 10$, so the difference could be real. However, the velocity field in the $\mathrm{Pr} = 10$ calculations was slightly different from that which existed for $\mathrm{Pr} = 1$ because a grid with a higher resolution was used.

The results in Fig. 16 show that the turbulent diffusivities for $\mathrm{Pr} = 1$, 3, 10 are approximately equal to the turbulent viscosity for $y_{\mathrm{w}} < 0.18H$ or $y_{\mathrm{w}} < 28$ wall units. A comparison of the maximum ν^{t} with the maximum D^{t} for $\mathrm{Pr} = 1$ gives a turbulent Prandtl number approximately equal to 0.87 in the center regions of the channel. This is somewhat larger than what has been obtained in calculations for heat transfer from two walls at the same temperature (Antonia and Kim, 1991). This suggests that Pr^{t} could depend weakly on the boundary conditions for the heat transfer and, perhaps, on the Reynolds number.

Fig. 17 shows the limiting behavior of D^{t}/y^3. The value of D^{t}/y^3 decreases weakly with Pr as $y_{\mathrm{w}} \to 0$. It is also noted that the thickness of the region, where D^{t}/y^3 is constant, decreases with increasing Pr, which suggests that this region would be

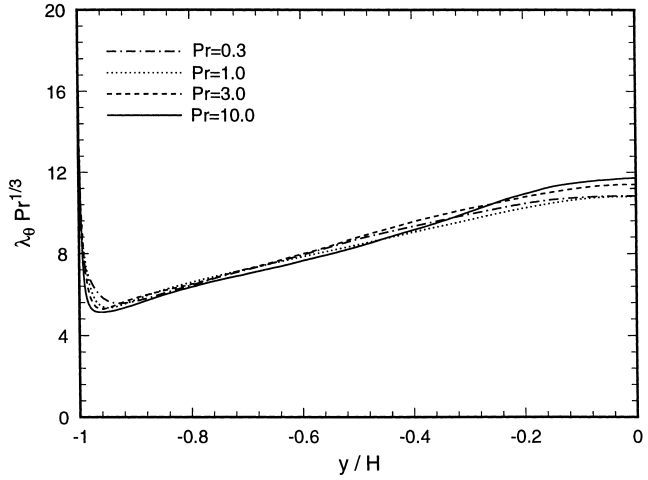

Fig. 15. Comparison of $\lambda_\theta \mathrm{Pr}^{1/3}$ at different Pr.

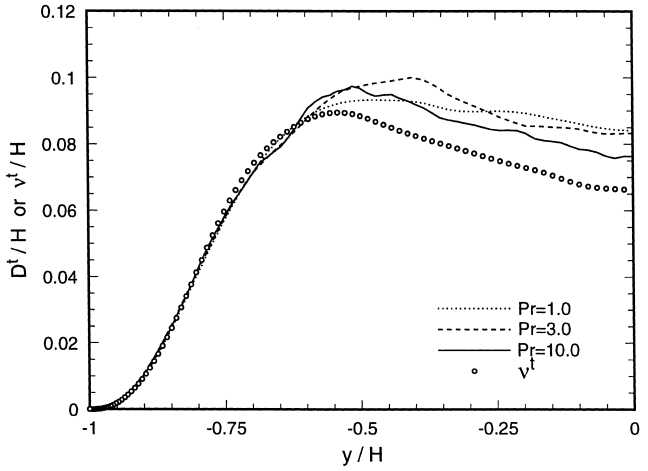

Fig. 16. Turbulent diffusivity.

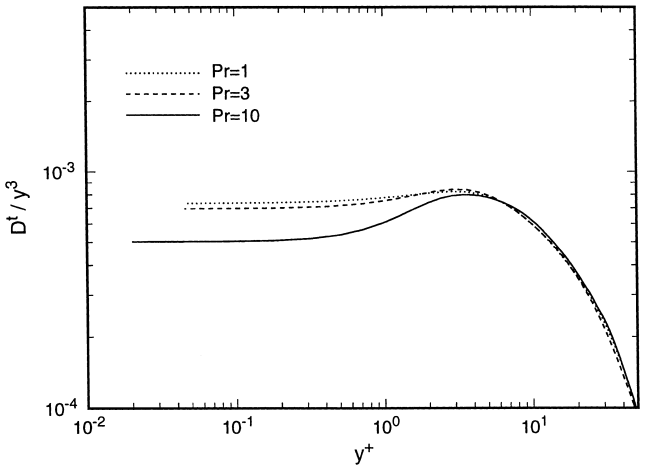

Fig. 17. Limiting behavior of turbulent diffusivity.

buried in a very thin conductive sublayer or would disappear in the limit of very high Pr. Since the contribution from turbulent transport is very small compared to that of molecular transport in this sublayer, the effect of turbulent motion for $y \to 0$ does not influence the mean temperature profile for very large Pr and the approach of assuming $D^t \sim y_w^3$ may not be correct.

The balance of turbulent kinetic energy, k, has a term, ϵ, which represents the rate of energy dissipation. A bulwark of k–ϵ models and Reynolds stress closure models is the definition of a characteristic time scale, τ, by using $\epsilon = k\tau^{-1}$ as a model for ϵ. In the k–ϵ model the turbulent viscosity is taken as $v^t \sim k\tau \sim k^2/\epsilon$. In attempts to use the temperature balance equation to model D^t, an additional time scale, τ_θ has been introduced, which is defined as $\tilde{\epsilon}_\theta = k_\theta \tau_\theta^{-1}$. Assumptions that $D^t \sim k\tau_\theta$ or $D^t \sim k(\tau_\theta \tau)^{1/2}$ have been made (Nagano and Kim, 1988). Calculated τ_θ are plotted in Fig. 18 for Pr = 0.3, 1, 3, 10. Values of τ, calculated from the velocity field with a $128 \times 193 \times 128$ grid, are also presented. Time scale τ_θ is seen to be strongly affected by Pr and to have a different shape from τ. Since λ_θ varies as $\mathrm{Pr}^{-1/3}$, it follows that $\tau_\theta \sim \mathrm{Pr}^{1/3}$. This suggests that the model for $\tilde{\epsilon}_\theta$ is flawed unless the effect of Pr on τ_θ can be explained more easily than the effect of Pr on $\tilde{\epsilon}_\theta$. Furthermore, relations for D^t of the type given above are inconsistent with the results in Fig. 16 which show a small effect (if any) of Pr on D^t.

The gradient transport model has also been used to calculate the turbulent convection of k_θ, by assuming

$$\overline{u_i\theta^2} = D^t \frac{\partial \overline{\theta^2}}{\partial x_i}. \tag{18}$$

Values of $\overline{\theta^2 v}$ are presented in Figs. 19 and 20 for Pr = 1 and 10. The curves are plots of $D^t(\mathrm{d}\overline{\theta^2}/\mathrm{d}y)$. It is seen that the model is fundamentally incorrect (as would be expected). Locations at which $\overline{v\theta^2} = 0$ do not correspond to a location where $\partial\overline{\theta^2}/\partial x_i = 0$. However, there is a rough agreement in the locations of maxima in $\overline{v\theta^2}$ and $D^t\partial\overline{\theta^2}/\partial y$.

6. Conclusion

For Pr $\geqslant$ 1 and for $y_w > 5$, the influence of Prandtl number on D^t is quite small. However, large effects of Pr on $\overline{u_i\theta}/(\overline{u_i^2})^{1/2}(\overline{\theta^2})^{1/2}$, $\overline{\theta^2}$, τ_θ and λ_θ are observed. This can be un-

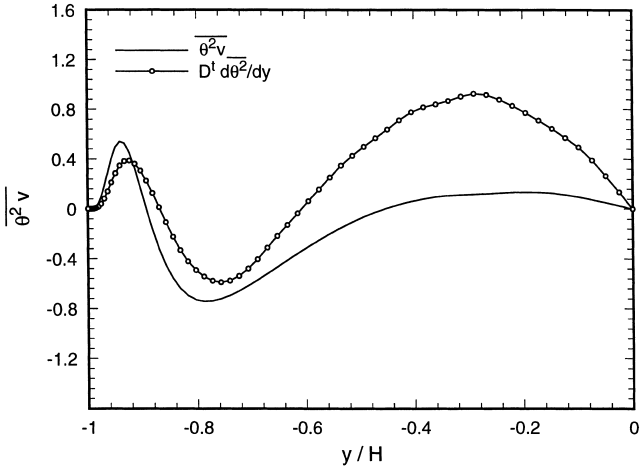

Fig. 19. Test of gradient diffusion model for turbulent transport term at Pr = 1.

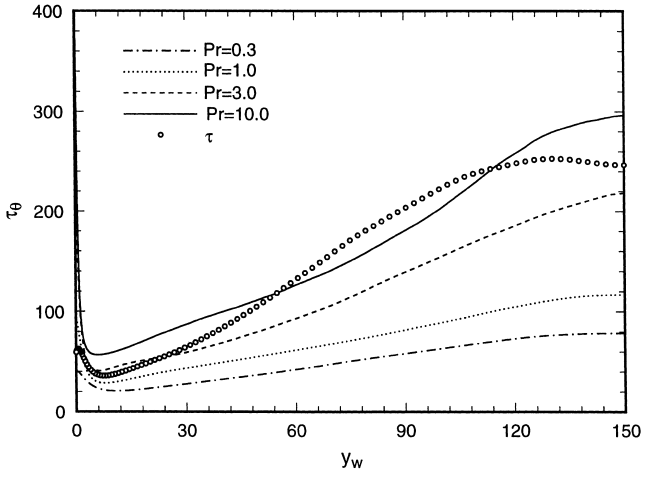

Fig. 18. Time scale of temperature field in wall unit.

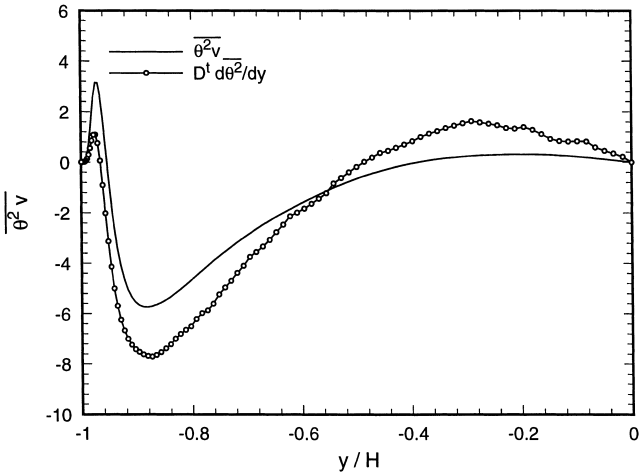

Fig. 20. Test of gradient diffusion model for turbulent transport term at Pr = 10.

derstood by recognizing that the range of wavenumbers associated with the fluctuating temperature field increases with Pr. At large Pr the spectral function for $\overline{\theta^2}$ can extend to wavenumbers for which the spectral functions for the velocity field are close to zero (Batchelor, 1967; Tennekes and Lumley, 1972). However, the correlation between the velocity and temperature fluctuations is determined by a range of wavenumbers which is approximately independent of Pr. These results suggest that τ, rather than τ_θ is a more significant time scale characterizing turbulent transport of heat. (This seems to be what was suggested by Horiuti, 1992.) A corollary of this observation is that the use of a turbulent Prandtl number to relate scalar transport to the velocity field could be a sensible approach. In fact, the assumption that $D^t = \nu^t$ is a good approximation for the viscous wall region (beyond $y_w = 5$) and the log layer. In the outer flow, $D^t > \nu^t$ and the turbulent Prandtl number depends on the boundary conditions. The Lagrangian methods developed by Papavassiliou and Hanratty (1995, 1997) could provide an opportunity to explore these effects.

For $Pr = 1$ the turbulent Prandtl number is unity for $y_w < 5$. At small y_w the turbulent diffusivity increases as y_w^3 for all Pr. However, D^t/y_w^3 decreases weakly with increasing Pr as $y_w \to 0$. This can be understood if it is recognized that temperature fluctuations in this region are mainly governed by fluctuations in the rate of heat transfer at the wall, rather than hydrodynamic mixing of hot and cold fluid (Shaw and Hanratty, 1977).

The thickness of the region where $D^t \sim y_w^3$ decreases with increasing Pr. However, it always lies in the conductive sublayer where turbulent transport is negligible compared to molecular transport; that is, turbulent effects in this region are not directly influencing the mean temperature profile. For very large Pr almost all of the temperature change occurs in the viscous sublayer where $\nu^t \sim y_w^3$. Because of this, the argument is commonly made that temperature or concentration profiles can be calculated by assuming $D^t \sim y_w^3$. The results outlined above suggests that this approach is incorrect.

If D^t is known, the dependency of $\overline{\theta^2}$ on y and on Pr can be calculated from the balance equation for k_θ, but expressions for the dissipation and transport terms are needed. The dissipation can be represented by Eq. (13). For the range of Pr covered by the Eulerian calculations, λ_θ varies roughly with $Pr^{-1/3}$. The explanation of this dependency resides in understanding the effect of Pr on the spectral function for $\overline{\theta^2}$. The use of the gradient transport model, Eq. (18), gives only a crude representation of the turbulent transport of k_θ. An examination of the transport terms for $Pr = 1$ and 10 suggests that the introduction of a proportionality constant in Eq. (18) will not provide a quick fix. However, the transport terms are not large, so even a rough approximation might be satisfactory.

Acknowledgements

This work is being supported by the National Science Foundation through grant CTS-95-03000. Computer resources have been provided by the National Center for Supercomputer Applications (NCSA), Urbana and the Computing Center at University of Kentucky, Lexington.

References

Antonia, R.A., Kim, J., 1991. Turbulent Prandtl number in the near-wall region of a turbulent channel flow. Int. J. Heat Mass Trans. 34 (7), 1905–1908.

Batchelor, G.K., 1967. Small-scale variation of convective quantities like temperature in a turbulent fluid: part 1. J. Fluid Mech. 5, 113.

Campbell, J.A., Hanratty, T.J., 1983. Mechanism of turbulent mass transfer at a solid boundary. A.I.Ch.E. Journal 29, 221.

Hanratty, T.J., Vassiliadou, E., 1988. Turbulent transfer to a wall at large Schmidt numbers. In: Hirata and Kasagi, N. (Eds.), Transport phenomena in turbulent shear flows. Theory, Experiment and Numerical Simulation, Hemisphere, New York, pp. 255–274.

Horiuti, K., 1992. Assessment of two-equation models of turbulent passive-scalar diffusion in channel flow. J. Fluid Mech. 238, 405–433.

Johnk, R.E., Hanratty, T.J., 1962. Temperature profiles for turbulent flow of air in a pipe-I. The fully developed heat transfer region. Chemical Eng. Sci. 17, 867–879.

Kasagi, N., Ohtsubo, Y., 1993. Direct numerical simulation of low Prandtl number thermal field in a turbulent channel flow. Turbulent Shear Flow 8, 97–119.

Kawamura, H., Abe, H., 1998. DNS of turbulent heat transfer in channel flow with respect to Reynolds number effect. Proceedings of the 2nd EF Conference in Turbulent Heat Transfer 1, 1.15–1.22.

Kawamura, H., Ohsaka, K., Yamamoto, K., 1997. DNS of turbulent heat transfer in channel flow with low to medium-high Prandtl number fluid. Proceedings of the 11th Symposium Turbulent Shear Flow 1, pp. 8.7–8.12.

Kim, J., Moin, P., 1989. Transport of passive scalars in a turbulent channel flow. Turbulent Shear Flow 6, 85–96.

Kontomaris, K., Hanratty, T.J., 1994. Effect of molecular diffusivity on point source diffusion in the center of a numerically simulated turbulent channel flow. Int. J. Heat Mass Trans. 37, 1817–1828.

Kontomaris, K., Hanratty, T.J., McLaughlin, J.B., 1992. An algorithm for tracking fluid particles in a spectral simulation of turbulent channel flow. J. Comput. Phys. 103, 231–242.

Launder, B.E., 1978. In: Bradshaw, P., Heat and Mass Transport in Turbulence. Springer, Berlin, pp. 231–287.

Launder, B.E., Samaraweera, 1979. Application of a second-moment turbulence closure to heat and mass transport in thin shear layer flows-I. Two-dimensional transport. Int. J. Heat Mass Trans. 22, 1631–1643.

Lyons, S.L., Hanratty, T.J., McLaughlin, J.B., 1991. Large-scale computer simulation of fully developed turbulent channel flow with heat transfer. Numer. Methods with Fluids 13, 999–1028.

Nagano, Y., Kim, C., 1988. A two-equation model for heat transport in wall turbulent shear flow. J. Heat Trans. 100, 583–589.

Nagano, Y., Tagawa, M., 1988. Statistical characteristics of wall turbulence with a passive scalar. J. Fluid Mech. 196, 157–185.

Nagano, Y., Tagawa, M., 1990. A structural turbulence model for triple products of velocity and scalar. J. Fluid Mech. 215, 639–657.

Papavassiliou, D., Hanratty, T.J., 1995. The use of Lagrangian methods to describe turbulent transport of heat from a wall. Industrial Eng. Chem. Res. 34, 3359–3367.

Papavassiliou, D., Hanratty, T.J., 1997. Transport of a passive scalar in a turbulent channel flow. Int. J. Heat Mass Trans. 40 (6), 1303–1311.

Shaw, D.A., Hanratty, T.J., 1977. Turbulent mass transfer to a wall for large Schmidt numbers. A.I.Ch.E Journal 2, 28–37.

Subramanian, C.S., Antonia, R.A., 1981. Effect of Reynolds number on a slightly heated turbulent boundary layer. Int. J. Heat Mass Trans. 24 (11), 1833–1846.

Tennekes, H., Lumley, J.L., 1972. A first course in turbulence. The MIT press, Cambridge.

Wikstrom, P.M., Johansson, A.V., 1998. Proceedings of the 2nd EF Conference in Turbulent Heat Transfer 1, 6.46–6.51.

Youssef, M.S., Nagano, Y., Tagawa, M., 1992. A two-equation heat transfer model for predicting turbulent thermal fields under arbitrary wall thermal conditions. Int. J. Heat Mass Trans. 35 (11), 3095–3104.